Analysis of Antenna's Location on Trains for Mobile Communications

Tomás Ferreira Duarte, Luís M. Correia
Instituto Superior Técnico / INOV-INESC
University of Lisbon
Lisbon, Portugal
tomas.duarte@tecnico.ulisboa.pt,
luis.m.correia@tecnico.ulisboa.pt

Fernando Santana
Thales
Lisbon, Portugal
fernando.santana@thalesgroup.com

Abstract — **The main objective of this work was to analyze the performance of antennas on trains for mobile communications, using dedicated communication systems. The work included the design of several 3D models using AutoCAD, as well as the use of antenna models based on real equipment used in the industry. The resulting combination of the train and antenna models was then used in the simulation of the propagation, through the CST Microwave Studio software, which takes into account antennas parameters and physical constraints imposed by the train roof. The main aspects considered concerning the placement of the antenna were roof aspects, essentially the longitudinal grooves, as well as the height of the antennas in the roof. The systems tested were TETRA, GSM-R, LTE-R and BBRS, with frequencies ranging from 400 MHz to 5.9 GHz. The study of the grooves impact allowed to conclude the higher frequencies suffer more severe impacts, with reductions in gain that can reach 14 dB for some angles, which was expected due to the wavelength being closer to the groove dimensions. At 400 MHz, it is recommended the antenna is placed in close proximity to the train roof, at 1 cm, while for higher frequencies the performance is improved with the increase in height to 20 cm. Depending on system requirements, a safety communications margin is recommended for some of the systems, ranging from 5 dB to 14 dB, taking into account if critical communications rely on the system.**

Keywords - Railway communications, antenna placement, longitudinal grooves, elevated plane.

I. INTRODUCTION

Mobile communications have been significantly evolving for the past decades both technically and concerning services provided. Following previous analogical systems, 2G was the first fully digital mobile communication system, launched in the early 1990s with a maximum data rate of 2.4 kbps.

Several standards emerged from 2G, the most common being the Global System for Mobile Communications (GSM), which was the first widely adopted standard, as it allowed for international roaming to become universal. GSM uses Time Division Multiple Access (TDMA), allowing up to 8 calls per channel in the 900 and 1800 MHz bands, using circuit switching, and being capable of data transmissions with a speed up to 9.6 kbps [1]. As of today, due to the significant improvements that have been made throughout the years, GSM is still the global standard for mobile communications.

Around the same time, railway operations were also subject to modernisation. In fact, by the end of the XX century, the European Rail Traffic Management System (ERTMS) was developed in the EU. This new system had the goal of improving railway business competitiveness and operational efficiency through standardisation across Europe.

As a result, 32 countries partnered with the worldwide railway organisation, the Union Internationale des Chemins de Fer (UIC), on the specification of a European standard for train control and communication systems. The goal was to eliminate conflicting rail operation rules and to define common homologation standards regarding traffic organization, rail gauge, electrification systems and communication systems [2].

ERTMS features several sub-standards, from which the most relevant for this work is GSM-R: a radio system designed to provide voice and data communications between the track and the train. This technology was developed based on regular GSM, with the inherent economies, but using specific frequencies [2]. GSM-R specifications were finalised by 2000, as a result of the European Integrated Radio Enhanced Network (EIRENE) and the Mobile Radio for Railway Networks in Europe (MORANE) protocols.

As GSM-R became the world standard for train communications, Terrestrial Trunked Radio (TETRA), another private mobile communication network, has become popular with underground rail services and other mission-critical forces such as emergency services, relying on lower frequencies, which allow for longer range cutting infrastructure costs. As a drawback, data transfer achieves a lower data rate [4].

BBRS, on the other hand, is a mobile communication solution provided by Thales mainly focusing on data transfer between railway infrastructures (railway stations, command centres) and rolling stock. In opposition to other systems, BBRS is focused on data transmission from its core, and therefore is the best suited

solution to data-heavy transmission systems such as video-surveillance or operational systems such as ERTMS [5].

As the first decade of the XXI century went on, mobile communications developed at a faster pace, giving birth to 3G and 4G, an evolution fuelled by mobile's ever-increasing popularity. By 2017, an estimated 5 billion devices were connected to mobile communications networks [6].

Railway operators are also in need of higher data rates and more capacity for train communications, leading to the development of improved systems such as LTE-R, based on commercial 4G. While it was already deployed in pioneer networks in Asia, LTE-R was not yet standardised by ETSI.

Operation of rail-dedicated mobile communication systems takes place just like regular GSM networks: trains are the moving users, featuring antennas on rolling stock's roof, which communicate with base station masts placed close to the railway.

The goal of this work was to analyse the performance of antennas mounted on trains for mobile communications, evaluating the influence of their position on the train roof. Different types of roof designs and other relevant factors affecting performance were analyzed. Several common antennas in the industry were tested using simulation software Computer Simulation Technology (CST) Microwave Studio.

The paper is organised as follows: Section I – Introduction; Section II - State of the art; Section III – Models and simulator description; Section IV – Results' analysis; Section V – Conclusions.

II. State of the art

In this section, an overview of relevant research for this work is presented. Since the scope is antenna placing on train roofs for mobile communications, sources for this include works focusing on antennas in train roofs, but also cars and other vehicles with metallic roofs.

Both Kathrein [7] and Antonics GmbH [8] antenna manufacturers provide installation guides for outdoor train and bus antenna placement, addressing several guidelines on mounting position, sealing, painting and minimum distance to obstacles.

More generally, [9] provides an insight on distributed microstrip patch antennas mounted on a moving platform, featuring near omnidirectional antennas with high gain. By analyzing the far field radiation patterns of patch antennas mounted on moving platforms, this paper investigates the optimal location for the antennas, focusing on 900 MHz technology and using a car-like vehicle model.

In [10], the influence of conducting environments on antenna radiation patterns is studied, using as a model a vehicle structure with the antenna located in its roof's rear section. The simulations were performed using the CST software, analyzing the influence in the radiation pattern of corners and edges in the car roof, as well as the curved plane effect.

Siemens Mobility [11] developed a study of the impact on the performance of the several different types of antennas, taking also into account various types of train roofs including models featuring strengthening bars a curved surfaces. The report provides a summary of the minimum spacing needed between antennas and isolation of transceivers to comply with minimum standards for different technologies.

André Ribeiro's work [12] provides an assessment of the impact in propagation resulting from curved train roof surfaces and A/C units placed near the antennas. The thesis is focused on GSM-R, LTE-R and BBRS systems and was carried under the development of a train plus antenna model based on CST software, taking into account parameters from the antennas and from physical constraints of surrounding environment. The results are safety distances for antenna placement in train roofs featuring these two characteristics.

III. Models and simulator description

A. Model description

In Figure 1 the methodology followed is shown, defining the critical input parameters, how calculations/simulations are performed and the output key performance indicators.

This said, the model consists of the development, through Antenna Magus, of a working 3D model of the antenna one is planning to fit in a given train, to operate a specific railway communication system, followed by its placement in several locations on the model of the train carriage and subsequent simulation using CST Microwave Studio software.

The results provided by the software include the 2D and 3D radiation patterns, the Half-Power Beam Width, the reflection coefficient and the first side lobe level. With these properties, it is possible to evaluate how changes in the positioning of the antenna affect the overall system performance, as well as to measure the impact of the grooved surface and the higher placement using a metallic structure.

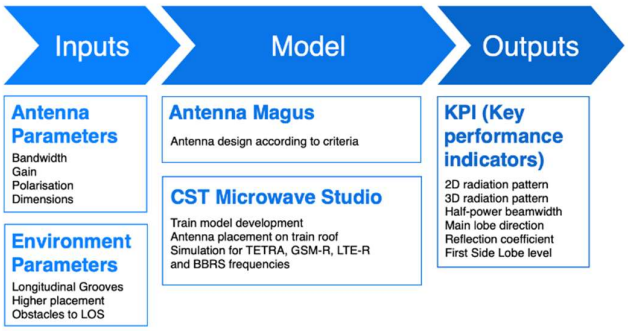

Figure 1. Model configuration.

Information provided from Thales related to their ongoing projects on mobile communications in railway networks helped define the main issues to address:

- First, the longitudinal metallic grooved surfaces in trains' roofs. While they are fitted for increased strength and durability, they might affect the radiation propagation of antennas placed there. Scattering might generate destructive interference and other multipath phenomenon degrading antenna performance. An example of such a surface can be seen in Figure 2.

Figure 2. Longitudinal grooves on train roof (from [13]).

- Then, the variation of the antenna height through the fitting of a metallic support structure on top of the train roof, potentially reducing impacts from objects placed in the train roof or its surface.

Following the definition of all input parameters of the model, simulations were performed through CST simulation software in order to understand the impacts caused by the different parameters. For that, 3D models of train roofs were designed to be fitted with antennas operating in the frequencies that correspond to each of the technologies in study.

Finally, CST outputs include results both allowing a qualitative impact analysis (3D and 2D radiation patterns) as well as quantitative analysis (half-power beam-width, main lobe direction, reflection coefficient and side lobe level), this last consisting of post-processing extracted data points from the patterns in order to come up with more accurate estimates for the impacts.

B. Train Model

In order to successfully achieve the goal of the work, one had to balance the model accuracy with the computational resources available. Hence, to simulate the behaviour of different antennas, a simplification of a train was made, focusing only on a single car roof, with a width of 3.5 m, 4 m of length and 0.340 m of height. The increase in the size of the model would not offer significant advantages for the evaluation of the antenna performance, since the goal is to assess the impact of grooved patterns in the propagation, in the close proximity of the antenna. Using a complete model of a train unit would allow to understand the impact of the whole rolling stock piece in the radiation pattern, but that result would not be relevant, since simulating 3 or 4 meters farther from the antenna placement location would have to include not only the train design pieces but also the surrounding scenario [12].

To address the first issue (impact of the groove patterns), defined in the previous section, three dimensions are relevant: groove height h_g, groove width w_g and distance between the grooves d_g (perpendicular to the length), as in Figure 3.

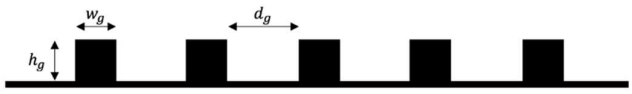

Figure 3. Longitudinal grooves – cross section.

Regarding the second issue (antenna & ground plane height) one has also three relevant dimensions: elevated ground plane width w_p and length l_p, and height regarding the train roof h_p, as in Figure 4. For simulation purposes, since in real-life the platform supports are usually made of dielectric material, these are not fitted, resulting in the antenna & ground plane being placed to a specific height regarding the roof, with no support.

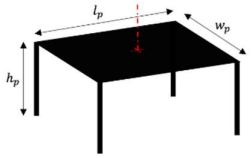

Figure 4. Elevated ground plane for antenna placement.

To validate the design of the grooves accurately, a wide research was done on the topic, however it was not possible to find relevant information on the dimensions of the strengthening bars on train rolling stock. To solve this problem, measurements were made to get factual data. Two different types of rolling stock were measured, on the 18th of March 2019 at Santa Apolónia railway station, with the results shown in Table 1.

Table 1. Rolling stock longitudinal grooves measurements.

Sorefame/Corail Intercity 1st class car	
Groove width (w_g)	12 mm
Distance between the grooves (d_g)	20 mm
Groove height (h_g)	23 mm
Sorefame UTE class 2200 electric multiple unit	
Groove width (w_g)	21 mm
Distance between grooves (d_g)	21 mm
Groove height (h_g)	13 mm

Due to the wide range of groove dimensions that was possible to observe, this work includes an analysis on the resulting impact from changing the groove dimensions. An initial base model was designed to serve as a basis to analyze the impact of the grooves: a rectangular, flat box of PEC material with the aforementioned dimensions. Then, straight and curved-shaped 3D models were designed and fitted with grooves, as it will be explained in detail in the Scenarios description section.

All the 3D model development work was done using Autodesk AutoCAD 2019. In Figure 5 it is possible to see the full (a) and detail view (b) of the curved grooved train model.

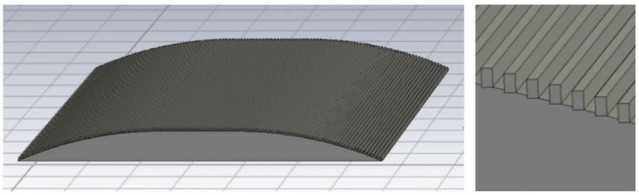

(a) Model overview (b) Detail

Figure 5. Curved grooved train model.

C. Key Performance Indicators

Following the model development, it is important to define the KPIs that help in addressing the main topics of this work. From the model configuration one has the main indicators:

- The 2D radiation patterns provided by CST allow a comprehensive analysis of the farfield power radiated by the antenna, and can be presented in a 2D graph with θ and ϕ coordinates but also in polar coordinates, allowing different cuts for both elevation and azimuth planes, with the possibility to have the data points extracted to develop further quantitative analyses;
- The 3D radiation pattern is also generated by CST and allows a qualitative overview of the global changes introduced by each of the scenarios under simulation, indicating the gain;
- The half-power beam width along with the main lobe direction and the side lobe level allow to understand the directivity of the antenna in the specific scenario, which is important since not all angles matter equally for the performance of the overall system;
- The reflection coefficient is an important measure of how well-adapted the antenna is.

In order to understand in more detail the impacts caused by the surfaces, the farfield polar plots are exported from CST in both planes $\theta = 90°$ and $\phi = 90°$, and the farfield gains for the two grooved surfaces compared in the relevant angle window. The angles acquired to compute the attenuations are depicted in

green in Figure 6, as well as the relevant angles (those in which is relevant to assess the impact of the grooved surfaces as they are the most critical for performance in a railway context).

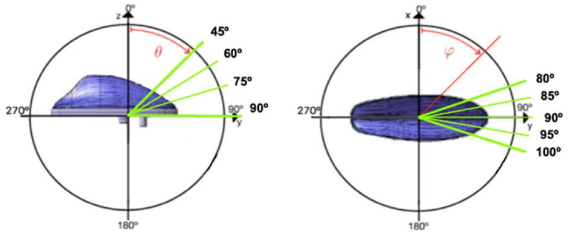

(a) Fixed azimuth ϕ=90 (a) Fixed elevation θ=90

Figure 6. Relevant angle window and acquisition angles.

From the main lobe direction (θ_{max}) and half-power beam width (α_{3dB}) metrics it is possible to compute the minimum ($\theta_{3dB-[°]}$) and the maximum ($\theta_{3dB+[°]}$) angles in which the main lobe radiates with at least half of the gain through:

$$\theta_{3dB-[°]} = \theta_{max\,[°]} - \frac{\alpha_{3dB\,[°]}}{2} \quad (1)$$

$$\theta_{3dB+[°]} = \theta_{max\,[°]} + \frac{\alpha_{3dB\,[°]}}{2} \quad (2)$$

With these two angles the interval in which at least half of the gain is radiated, Θ_{3dB}, is defined:

$$\Theta_{3dB\,[°]} = \left[\theta_{3dB-[°]}; \theta_{3dB+[°]}\right] \quad (3)$$

This measure will be useful to assess if the grooved surfaces change the radiation pattern in a way that impacts severely the radiation in the window of relevant angles. Additionally, gain differences from polar plots are given by:

$$\Delta G_{[\mathrm{dB}]}(\theta,\phi) = G_{gro\,[\mathrm{dBi}]}(\theta,\phi) - G_{fla\,[\mathrm{dBi}]}(\theta,\phi) \quad (4)$$

where:

- G_{gro} is the gain for the grooved surface (straight or curved), acquired from the CST polar plot farfield result for a specific co-elevation and azimuth angle pair;
- G_{fla} is the gain for the flat surface acquired from the CST polar plot farfield result for a specific co-elevation and azimuth angle pair.

Furthermore, with the angles acquired from the polar plots a mean attenuation can also be computed, through the following general expression:

$$\overline{\Delta G_{[\mathrm{dB}]}(\theta,\phi)} = \frac{1}{N_{ang}} \sum_{n=1}^{N_{ang}} \Delta G_{n\,[\mathrm{dB}]}(\theta,\phi) \quad (5)$$

where:

- N_{ang} is the number of angles used for the sampling;
- $\Delta G_{n\,[\mathrm{dBi}]}(\theta,\phi)$ is the gain difference for the angle n.

Using the results from CST, a mean gain difference can be calculated for $\phi = 90°$ (46 angles):

$$\overline{\Delta G_{[\mathrm{dB}]}(\theta,\phi=90°)} \quad , \quad N_{ang} = 46 \quad (6)$$

Similarly, the resulting gain difference for a fixed co-elevation of $\theta = 90°$ (21 angles) is given by:

$$\overline{\Delta G_{[\mathrm{dB}]}(\theta=90°,\phi)} \quad , \quad N_{ang} = 21 \quad (7)$$

Additionally, and specially for lower frequencies, due to track morphology and the longer range at these frequencies, BS might be placed in an elevation or surrounding vantage point instead of the trackside [14]. Due to this, it is also relevant to compute the average gain for all angles, which consists in using equation (5) with $N_{ang} = 360$.

D. Model assessment

To assess the validity of the model the flat roof surface was first tested for all the four frequencies to serve as starting point. The farfield view for the 2.6 GHz antenna with the PEC box flat surface can be seen in Figure 7, featuring a gain of 7.7 dBi. The reflection coefficient is acceptable at the central frequency for 2.6 GHz, as can be seen in Figure 8.

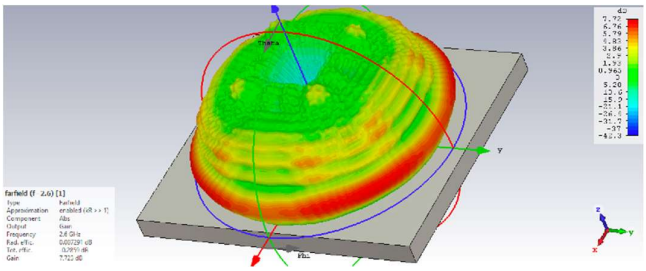

Figure 7. Farfield view – flat model with a 2.6 GHz monopole.

For the rest of the frequency range in test the results were similar, corresponding to an increase in gain due to the increased PEC surface and higher directivity, which is more subtle in the lower frequencies and shows a bigger impact for the higher ones.

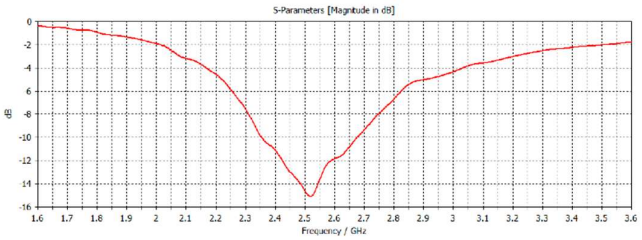

Figure 8. Reflection coefficient – flat model with a 2.6 GHz monopole.

In Table 2 it is possible to see the attained results for all frequencies, with the cutting plane set for $\phi = 90$, meaning a cut along the train in forward direction. The PEC box used is the same for all four antennas.

Table 2. Antenna parameters with a flat surface at $\phi = 90°$.

Technology	TETRA	GSM-R	LTE-R	BBRS
f [MHz]	400	900	2600	5900
G [dB]	6.0	6.6	7.7	6.7
S_{11} [dB]	-13.1	-15.5	-11.9	-18.8
ML_{width} [dB]	5.1	5.8	6.3	6.0
α_{3dB} [°]	31.3	19.8	12.3	13.5
S_{LL} [dB]	-4.7	-2.5	-2.2	-0.9

The angular width shows a significant decrease in the higher frequencies, with the side lobe level magnitude being higher in the lower end of the frequencies. It is then possible to conclude the higher frequency antennas have a higher directivity, with all systems achieving a similar total efficiency. The Main Lobe Width (ML_{width}) was consistent across all frequencies.

IV. RESULTS' ANALYSIS

A. Scenarios description

First, one defines the reference scenario for the problem under study: this consists in the most realistic approach for the problem, which is a train featuring a curved, grooved roof, with the antenna being placed 1 cm above the surface (h_p=1 cm), supported in a plastic support that is not featured since the dielectric properties of the plastic do not impact propagation.

The model for this scenario, sized to offer the best trade-off between simulation accuracy and computational resources used, can be seen in Figure 9 and was fitted with medium-sized grooves with the following dimensions:

- Groove width w_g = 15 mm;
- Groove height h_g = 25 mm;
- Distance between grooves d_g = 15 mm.

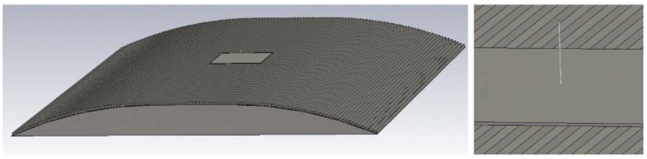

(b) Model overview (b) Detail

Figure 9. Reference scenario featuring a 900 MHz antenna.

The first approach addresses the influence of the grooved surface in the performance of the antennas. For that, as explained before, three 3D models are used: a flat box of PEC material, depicting a section of a real train roof; a straight grooved model, with the same dimensions and finally the reference curved grooved model.

For this approach, the procedure consists in testing the antennas for the four frequencies (400, 900, 2600 and 5900 MHz) placed on the three models, to compare the differences introduced by the grooves and the curved surface to the antenna behavior placed on top of the flat surface. No inputs should be changed for theses simulations comparing to the isolated antennas tests, unless mismatch occurs and additional tuning is required.

For the flat model, the ground plane of the monopoles is placed 1 cm above the top, while for the grooved models the ground plane is placed 1 cm above the highest groove surface (h_p=1 cm). In what concerns the meshing, dedicated meshing groups for the port, the antenna wire, and its ground plane are kept, while the global mesh properties are adjusted, for the different frequencies and 3D models, to always guarantee an adequate number of mesh cells (between 5 and 10 million mesh cells), with the heaviest simulations being the 5.9 GHz ones due to the lowest wavelength.

The next approach has the goal of understanding how the groove dimensions impacts the performance, as there is not a common groove size. Hence, the curved grooved model depicted above was changed:

- Wider groove width w_g = 20 mm (instead of 15 mm);
- Smaller groove height h_g = 15 mm (instead of 25 mm);
- Grooves farther from each other with a distance between them d_g = 20 mm (instead of 15 mm).

For this approach, only the position of the antenna ground plane is adjusted, to cope with the decrease in the grooves height (and to sit 1 cm above its top, as in the reference scenario). The results are then compared with the reference grooved scenario.

Finally, as stated before, in order to evaluate the impact of the antenna height in the performance, additional simulations are done, changing the antenna and ground plane height (h_p).

While most of the railway antennas are placed close to the train roof, some are elevated to – supposedly – improve its performance, at a height usually no higher than 20 cm, since one has to take into account the monopole size (the TETRA antenna designed has 16.5 cm, for instance). Previous work [12] tested several scenarios including air conditioning units with a 45 cm height on the rooftops, hence elevating the top of the monopole to close to 40 cm is quite reasonable. The range of heights is defined in Table 3, where a comparison with the wavelengths for the different frequencies is made. It is possible to see that, for the lower frequencies, the range of heights considered is far from the wavelength, whereas for the higher frequencies one has the opposite case. It is therefore expected that the higher frequencies experience more significant impacts from the changes in antenna height.

Table 3. Comparison of antenna heights with wavelengths.

Frequency [MHz]		**400**	**900**	**2600**	**5900**
Wavelength [m]		**0.75**	**0.33**	**0.12**	**0.05**
Antenna height [m]	h_p=0.01	0.01λ	0.03λ	0.09λ	0.20λ
	h_p=0.10	0.13λ	0.30λ	0.87λ	1.97λ
	h_p=0.20	0.27λ	0.60λ	1.73λ	3.93λ

B. Influence of the grooved surface

In the first approach, the four antennas were tested for the flat PEC model, the straight grooved model and the reference scenario curved grooved model. It is important to remember the most important KPI will be the gain, which will help understanding how the grooved surface impacts the expected performance of the train antenna, and in which directions.

The first simulations were performed for 400 MHz, and the comparison done for the ϕ=90º plane according to the defined angles of interest for the problem. The results are in Table 4.

Table 4. Antenna performance at 400 MHz – different surfaces.

Surface	**Gain [dB]**	**ML_{dir} θ [º]**	**α_{3dB} [º]**	**S_{LL} [dB]**	**Θ_{3dB} [º]**
Flat	6.0	63	31.3	-4.7	[47;79]
Straight gro.	5.8	63	31.0	-0.5	[47;78]
Curved gro.	5.4	73	61.5	-1.1	[42;104]

The increase in the half-power beamwidth occurs due to the dispersion of electromagnetic performance caused by the curved surface of this model, and is quite significant (nearly doubles the beamwidth from 31.3º to 61.5º), meaning the curved grooved surface radiates a power higher than 2.7 dBi (half of maximum gain for an interval of $\theta \in [42; 104]°$ instead of $\theta \in [47; 79]°$ for the flat surface (with a slightly higher gain, however). Although this allows the main lobe to cover the relevant window of angles in terms of elevation, it also goes beyond the limits defined, meaning there is some power being radiated out of the defined boundaries, potentially reducing overall performance.

The 2D farfields for the reference, straight grooved and curved groove surface can be seen in Figure 10, Figure 11 and Figure 12, respectively.

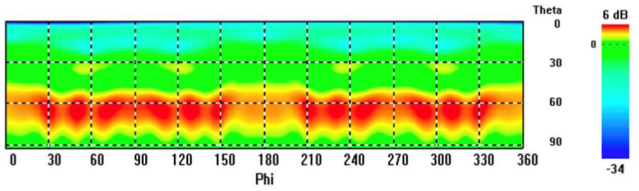

Figure 10. 400 MHz antenna farfield - flat surface.

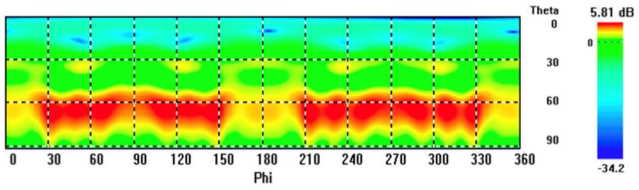

Figure 11. 400 MHz antenna farfield – straight grooved surface.

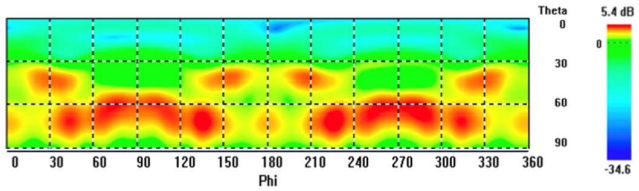

Figure 12. 400 MHz antenna farfield – curved grooved surface.

It can be clearly seen in the curved surface farfield the dispersion caused by the shape of the surface, which increases the directivity of the antenna since the antenna is no longer quasi-isotropic but features an increased beam directivity, especially for ϕ between 60 and 120 degrees.

On the other hand, the radiation pattern shows a clear decrease in power for the side views (ϕ=0º and ϕ=180º), which is not expected to impact performance of the overall system since the radiation in these angles will only be considered when the train is passing by a BS and, in that situation, due to the proximity of the antennas, the attenuation does not pose a threat to the link.

Looking at the results shown, one can see the biggest changes occur not for the straight grooved surface but when besides the grooved surface, a curved shape is also added. While the gain does not change significantly, the main lobe direction is lowered from 63º to 73º, closer to the horizon.

For the 900 MHz antenna, the same procedure was followed, testing the antenna for the three surface models. The results can be seen in Table 5.

Table 5. Antenna performance at 900 MHz – different surfaces.

Surface	Gain [dB]	ML_{dir} θ [º]	α_{3dB} [º]	S_{LL} [dB]	Θ_{3dB} [º]
Flat	6.6	74	19.8	-2.5	[64;84]
Straight gro.	7.1	73	19.2	-3.3	[63;83]
Curved gro.	6.6	89	25.7	-1.7	[76;102]

From the results shown it is possible to observe a clear increase in the main lobe direction angle for the curved surface, and a significant α_{3dB} increase as well. The tilt of the main lobe should not have a significant influence in the system since it is now closer from the horizon but still inside the relevant angle interval. For the straight grooved surface there are no critical changes (1 degree tilt on the main lobe and a very slight decrease of α_{3dB} and S_{LL} values), which suggests the biggest impacts for the performance of the 900 MHz antenna come from the curved surface rather than the grooves.

The 2D farfields show a behavior very close to the 400 MHz antenna. The straight grooved surface shows some influence on the propagation, increasing its directivity towards the front and rear of the train (ϕ=90º and ϕ=270º) and decreasing the radiation on side angles. Furthermore, the increase in the α_{3dB} is not entirely positive for the relevant angle window, since while the gain does not decrease (compared to the reference flat surface), having α_{3dB}=25.7º and the main lobe direction increased to θ=89º means a gain higher than 3.3 dBi is radiated for an interval of $\theta \in [76; 102]°$ instead of $\theta \in [64; 84]°$ for the flat surface. Since the relevant window ends at $\theta = 90°$ it would most likely not be useful to radiate at a higher intensity for an elevation higher than that (lower than the horizon).

Similarly to the lower frequencies, for 2.6 GHz the same procedure was followed, with the antenna tested for the three models depicting the roof of the train. The results are in Table 6.

For this frequency it is immediately possible to see how the straight grooved surface changes significantly the main lobe direction from θ=79º to θ=56º, meaning the main lobe is tilted up, and since the half-power beamwidth increases to α_{3dB}=21.4º a gain higher than 3.8 dBi is radiated for an interval of $\theta \in [45; 67]°$ instead of $\theta \in [73; 85]°$ for the flat surface (with a lower gain, however). The curved grooved surface further rises the main lobe direction, and in addition to the smaller half-power beamwidth than the straight grooved surface, the resulting beam with gain higher than 4 dBi is radiated for $\theta \in [46; 62]°$.

Table 6. Antenna performance at 2.6 GHz – different surfaces.

Surface	Gain [dB]	ML_{dir} θ [º]	α_{3dB} [º]	S_{LL} [dB]	Θ_{3dB} [º]
Flat	7.7	79	12.3	-2.2	[73;85]
Straight gro.	8.8	56	21.4	-0.9	[45;67]
Curved gro.	8.0	54	15.5	-0.7	[46;62]

The 2D farfield of the flat surface is very similar to the lower frequencies' ones, while the straight grooved and curved grooved (Figure 13) surfaces feature a clear decrease of power for the 60-120º (and 240-300º) band in the azimuth plane, slightly stronger in the curved surface.

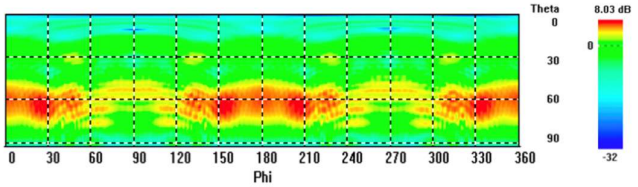

Figure 13. 2.6 GHz antenna farfield – curved grooved surface.

This poses a problem since the angles of interest for this plane are $\phi \in [80; 100]°$ because this represents the front of the train. From the figure one concludes that, for this frequency, a severe impact in the performance of the system is expected due to the strong attenuation in the propagation in the relevant angles for the link with the trackside BS. Since there is a significant change in the radiation pattern for this frequency, the 2D polar plot was also computed, and can be seen in Figure 14.

This last plot confirms the biggest gain decrease occurs for ϕ=90º (and, symmetrically, for ϕ=270º), with a relevant reduction for the straight grooved surface and much stronger for

the curved grooved surface (almost 10 dB). This impact is higher for 2.6 GHz than for the lower frequencies due to the size of the grooves being close to the wavelength.

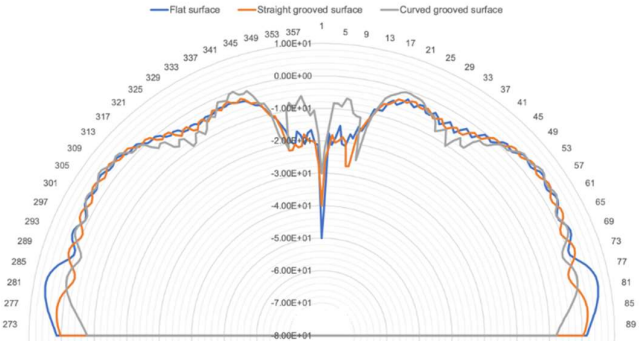

Figure 14. 2.6 GHz antenna polar plot – three surfaces.

Finally the 5.9 GHz antenna was tested for the same three scenarios. The results can be seen in Table 7. The first challenge was to tune once again the antenna for the new surfaces, since with the flat model the antenna was not operating correctly (S_{11} value increased to higher than -10 dB), hence it was needed to reduce the size of the monopole to h=10 cm.

Table 7. Antenna performance at 5.9 GHz – different surfaces.

Surface	Gain [dB]	ML_{dir} θ [º]	α_{3dB} [º]	S_{LL} [dB]	Θ_{3dB} [º]
Flat	6.7	75	13.5	-0.9	[68;82]
Straight gro.	5.7	73	16.1	-0.8	[66;81]
Curved gro.	7.6	49	16.7	-1.8	[41;57]

For this frequency there are no significant changes in the KPIs for the straight grooved compared to the flat surface, while for the curved grooved model one can see a noteworthy increase in the main lobe direction, pulling the main lobe half-power range up, with part of it getting outside the relevant angles. The 2D farfield for the curved groove surface can be seen in Figure 15 and shows a significant dispersion. All three farfields showed the grooved surfaces increase the dispersion of the radiated power, with the gain in the flat surface being more concentrated in the 60º to 75º band while for the grooved surfaces it is possible to observe there is no consistent band of angles with higher gain, while there are a lot of lobes in all directions.

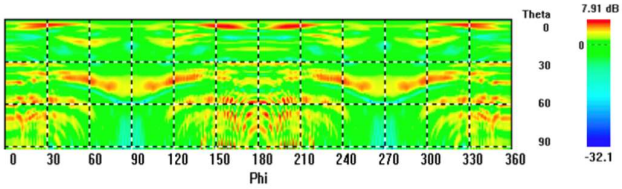

Figure 15. 5.9 GHz antenna farfield – curved grooved surface.

According to the equations for gain differences calculations presented previously, the overall differences for the acquisition angles were calculated for all frequencies. First, the equations for the straight grooved surface comparing to the flat surface are computed, both for $\phi = 90°$ and $\theta = 90°$ planes, followed by the same procedure for the curved grooved surface (reference scenario) comparing to the flat surface.

From the gain differences computed it was possible to draw some conclusions on the impacts generated by both the curved surface and the grooved surfaces:

- The lower frequencies (400 and 900 MHz) are the less impacted by the grooves, due to the wavelengths being far from the groove dimensions (the maximum relative size is h_g that is equal to 0.75λ for 900 MHz), and the computed average gain differences show a less than 1 dB gain reduction, hence no difficulties are expected for TETRA and GSM-R;
- The higher frequencies (2.6 and 5.9 GHz) show the introduction of the grooves causes a significant impact, especially in the angles around ϕ=90º, where the power decreases, an effect that is worse for the 2.6 GHz case, where average gain differences show an impact up to -14 dB in some angles. Strong impacts are expected and therefore, if an average approach is preferred, a 10 dB safety margin should be considered for LTE-R systems with grooved roof designs. Should the system support critical functions, then a worst approach safety margin should be used, considering a 14 dB safety margin;
- The 5.9 GHz simulations show a very disperse radiation pattern with a lot of lobes, and while on average the groove introduction did not worsen the gain, in some angles the gain was almost -14 dB lower for the grooved surface, which suggests a safety margin of communications should also be considered for BBRS. Although 5 dB would probably be enough to use as average safety margin, the worst approach should consider the same 14 dB.

C. Influence of the grooves dimensions

In the second approach the antennas were tested with the modified curved grooved model, featuring wider grooves (w_g = 20 mm) with a smaller height (h_g = 15 mm) and a bigger distance between them (d_g = 20 mm), and the KPI comparison was done with the reference curved grooved scenario.

For the 400 MHz antenna the results can be seen in Table 8 and show a slight decrease of the main lobe direction, which is for the wider grooved model now pointing upper, but a significant reduction of the half-power beamwidth, resulting in a narrower main lobe half-power range, that keeps, however, within the relevant angle window.

Radiation patterns show no significant changes except for the slight attenuation in the gain for the side views, (stronger than observed for the reference grooved model). It is possible to say the wider grooves impact more the side view, mostly due to higher reflection, but in an extension that shall not compromise the link to the BS (3-4 dB reduction).

Table 8. Antenna performance at 400 MHz – grooved surfaces.

Surface	Gain [dB]	ML_{dir} θ [º]	α_{3dB} [º]	S_{LL} [dB]	Θ_{3dB} [º]
Reference	5.4	73	61.5	-1.1	[42;104]
Wider grooves	5.3	62	29.7	0.5	[47;77]

For the 900 MHz simulation, the results (Table 9) show a slight decrease of the main lobe direction, which is for the wider grooved model now pointing upper, with an also slight reduction of the half-power beam width. These two effects combined, while reducing the size of the main lobe half-power interval Θ, put this range totally in the relevant angle window. This can generally be considered a positive impact.

The pattern shows a slight reduction in the dispersion, while maintaining the same profile that was observed for the reference scenario. There are no significant changes since the groove dimensions are far from the wavelength (λ=0.33 m) for both

models. The wider grooved surface suggests a higher gain should be expected for the 30 to $\phi \in [30; 140]°$ meaning it most likely improves the link to the BS.

Table 9. Antenna performance at 900 MHz – grooved surfaces.

Surface	Gain [dB]	ML_{dir} θ [º]	α_{3dB} [º]	S_{LL} [dB]	Θ_{3dB} [º]
Reference	6.6	89	25.7	-1.7	[76;102]
Wider grooves	6.4	73	19.5	-0.6	[63;83]

For the 2.6 GHz antenna the same procedure was followed, with the antenna tested for the model with wider grooves. The results are in Table 10, showing the change in the groove dimensions did not impact significantly the pattern or the KPIs.

Table 10. Antenna performance at 2.6 GHz – grooved surfaces.

Surface	Gain [dB]	ML_{dir} θ [º]	α_{3dB} [º]	S_{LL} [dB]	Θ_{3dB} [º]
Reference	8.0	54	15.5	-0.7	[46;62]
Wider grooves	7.8	54	15.1	-0.6	[46;62]

Finally the wider grooves model was tested for the 5.9 GHz antenna. Results are shown in Table 11, being possible to see a very strong reduction of the main lobe direction angle, together with a reduction to one third of the half power beam-width, meaning the main lobe is for the wider grooved model now pointing upward and is quite thinner, being now completely out of the relevant angle window. The farfield diagrams show a very scattered gain for both surfaces, with a slight reduction of the dispersion of the wider grooved model. In both models one can see that at ϕ=90º the gain is very low, which is very critical for the communications, since BBRS systems typically feature BS 300 m apart from each other and is therefore very likely these will be directly forward facing the train.

The significant impacts observed may be explained by, at 5.9 GHz, the wavelength being 0.05 m which is exactly in the range of the groove dimensions' changes, so it was expected changes in the groove size would impact severely the KPI in analysis.

Table 11. Antenna performance at 5.9 GHz – grooved surfaces.

Surface	Gain [dB]	ML_{dir} θ [º]	α_{3dB} [º]	S_{LL} [dB]	Θ_{3dB} [º]
Reference	7.6	49	16.7	-1.8	[41;57]
Wider grooves	9.9	4.8	5	-0.9	[4;9]

Once again the gain differences were computed, and it was possible to conclude:

- The lower frequencies (400 and 900 MHz) show a slight power decrease for the side view on the wider grooved surface, but not very significant (3 to 4 dB), while for 2.6 GHz no changes occur when the grooves are widened, therefore no further safety margins are recommended for these frequencies;
- The 5.9 GHz simulation continues to show a very disperse radiation pattern, being the frequency for which more changes happened, namely the decrease in the main lobe direction (from 49º to 5º) making it point almost vertically, but again, the pattern shows a lot of lobes, and the average gain differences show the impacts are under 1 dB on average. Since some specific angles feature gain losses of almost 9 dB comparing to the reference scenario, it is recommended that the 5 dB safety margin of communications is applied to any grooved roof train type, however the worst case approach should be now 23 dB to cope with the maximum gain decrease comparing to the flat scenario.

D. Influence of the antenna & ground plane height

Finally, the impact of the antenna height in the performance was evaluated. In addition to the reference scenario with the ground plane at 1 cm from the grooved surface top, further simulations with h_p=10 and h_p=20 cm were done.

For the 400 MHz antenna, the increase in the antenna & ground plane height has a significant impact in the KPIs. Looking at Table 12 it is possible to see the raise to h_p=10 cm improves the antenna gain while reducing the main lobe direction and the half-power beamwidth, meaning the main lobe points upwards and is thinner, with the Θ range out of the relevant angle window. The additional raise to h_p=20 cm further increases the gain, although not as strongly as with h_p=10 cm. On the other hand, the half-power beamwidth rises along with an improvement in the main lobe direction, which pushes the main lobe half-power range further down to be inside the relevant angle window, however only partially.

Table 12. Antenna performance at 400 MHz – three heights.

Height	Gain [dB]	ML_{dir} θ [º]	α_{3dB} [º]	S_{LL} [dB]	Θ_{3dB} [º]
h_p=1 cm (ref.)	5.4	73	61.5	-1.1	[42;104]
h_p=10 cm	7.7	33	18.6	-3.5	[24;42]
h_p=20 cm	7.9	44	46.7	-1.6	[21;67]

The 2D farfield for h_p=10 cm can be seen in Figure 16, where the impact of the height increase in the radiation patter is clear. With the increase of the antenna and ground plane height, the radiation stops "following" the curved surface to be more directional for specific angles. The gain increase observed in the table above results from a lower dispersion of the radiation. However, one can see that, for the relevant angles (around ϕ=90º) there is a clear decrease in radiated power for the higher placement scenarios, and is therefore possible to conclude this increase in height is not positive for this frequency.

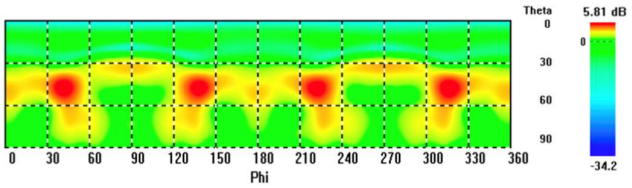

Figure 16. 400 MHz antenna farfield at h_p=10 cm.

For the 900 MHz simulations, the results (Table 13) showed a consistent decrease of the main lobe direction, along with a reduction of the half-power beamwidth, both these leading to a thinner, more elevated main lobe half-power interval. However, this tilting up might be considered beneficial since for h_p=1 cm part of this range was outside the relevant angle window, which does not happen for the two higher placement settings.

The 2D farfields show the increase of the antenna height results in significant changes in the radiation patterns, especially for the intermediate height where a strong power dispersion can be observed. For the proximities of ϕ=90º, there is lower radiation intensity. In the elevation plane, both scenarios (h_p=10

and h_p=20 cm) tilt the higher gains up, moving them to the range of θ=60º, which is still in the relevant angle window.

Table 13. Antenna performance at 900 MHz – three heights.

Height	Gain [dB]	ML_{dir} θ [º]	α_{3dB} [º]	S_{LL} [dB]	Θ_{3dB} [º]
h_p=1 cm (ref.)	6.6	89	25.7	-1.7	[76;102]
h_p=10 cm	6.4	79	18.9	-0.5	[70;88]
h_p=20 cm	6.6	59	12.1	-2.4	[53;65]

For the 2.6 GHz simulations, knowing the height changes are in the same order of greatness than the wavelength, significant changes were expected. Looking at Table 14 it is possible to see a tilt down of the main lobe occurs strongly for the highest placement, however all the three placements feature the main lobe half-power range within the relevant angle window. The half-power beamwidth reduces for the biggest h_p, while the side lobe level only shows slight changes.

Table 14. Antenna performance at 2.6 GHz – three heights.

Height	Gain [dB]	ML_{dir} θ [º]	α_{3dB} [º]	S_{LL} [dB]	Θ_{3dB} [º]
h_p=1 cm (ref.)	8.0	54	15.5	-0.7	[46;62]
h_p=10 cm	6.9	56	15.9	-0.5	[48;64]
h_p=20 cm	6.6	73	6.2	-0.7	[70;76]

The 2D farfields show (Figure 17 for hp=20 cm) the radiation power is more isotropically distributed as the height of the antenna increases, which is beneficial for the 60-120º (and 240-300º) band in the azimuth plane, which has now more power, and this is a very important band for the link to the BS as seen before. One can conclude the increase in height will probably improve performance of the system for this frequency.

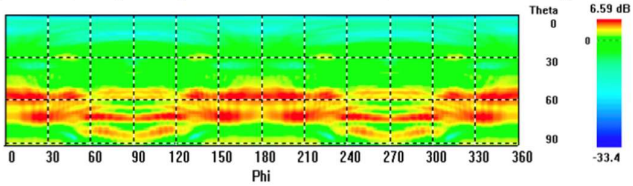

Figure 17. 2.6 GHz antenna farfield at h_p=20 cm.

Finally, for the 5.9 GHz simulations, as for 2.6 GHz, strong impacts were expected from the height changes, since they are in the range of the wavelength for this frequency.

Looking at the results (Table 15) it is possible to see an increase in gain with the increase in height of the antenna, but along with a strong reduction of the half-power beam width, meaning the higher the antenna, the more scattered is the power in the radiation pattern. With a 2.2º α_{3dB} it is not relevant to talk about main lobe. The 2D farfields confirm the radiation is quite scattered, and although the increase in height makes some changes in the pattern, it does not seem to impact strongly enough the relevant angle window.

Table 15. Antenna performance at 5.9 GHz – three heights.

Height	Gain [dB]	ML_{dir} θ [º]	α_{3dB} [º]	S_{LL} [dB]	Θ_{3dB} [º]
h_p=1 cm (ref.)	7.6	49	16.7	-1.8	[41;57]
h_p=10 cm	10.1	39	6.3	-1.2	[36;42]
h_p=20 cm	12.0	18	2.2	-1.6	[17;19]

Similar to previous approaches, gain differences were computed, comparing the increased heights (h_p=10 cm and h_p=20 cm) with the reference scenario (h_p=1 cm), hence it was possible to draw some conclusions on the impacts generated by both the changes in antenna & ground plane height:

- The 400 MHz, the impacts are mostly negative or neutral, with the increase in height consistently increasing the gain, but with a strong directivity for a range outside the relevant angle window. Gain differences computed show slight reductions or no changes in gain for both the relevant window and N_{ang}=360, therefore the recommendation for 400 MHz systems is to place the antenna closer to roof;
- In the 900 MHz patterns it was possible to see a gain penalty in the pattern for ϕ angles between 60 and 120 degrees for h_p=10 cm while the further increase to 20 cm created a consistent lobe facing forward, tilted up to θ=60º, which might very positive for BS placements far from trackside, depending on system requirements, suggesting 900 MHz systems should place the antenna the highest possible, closer to 20 cm to benefit the forward-facing propagation;
- This effect was similar for the 2600 MHz antenna, although in this case both increases in height were positive, with average strong gain improvements for almost all angles and windows, reaching more than 10 dB. Antennas for this system placed higher can reduce significantly the impacts caused by the grooved surface, as this frequency was the most affected by them. Since the negative impacts are reduced with the increase in height, it is hence recommended to, with an average safety approach, add no margin of communications, while for a worst case approach a 7 dB margin should be considered;
- The 5.9 GHz simulations showed a strong increase in gain, with a reduction of the half-power beamwidth, and a tilt up of the main lobe direction. Nevertheless, and since the radiation patterns for this frequency are quite disperse, the gain differences computed show a positive impact of around 4 dB for both heights, but the pattern still shows most gain is radiated for the side views. For this frequency it is, then, generally positive to increase the height of the antenna. The safety margin for the average approach can be avoided with the increase in height, while for the worst case approach a 10 dB margin should be used.

V. CONCLUSIONS

The goal of this work is to analyze the performance of antennas mounted on trains for mobile communications, evaluating the influence of their position on the train roof and the roof surface, more specifically two particular issues: the influence of a grooved surface in the antenna performance, and the influence of the antenna height. To assess this goal, a study on the train roof parameters was conducted, followed by the development of a general model. This model is considered to depict the train roof scenario in a reliable way, with dimensions that would allow the simulations to be accurate enough. The frequencies chosen were defined through the industry link. A wide range of simulations were executed through the CST Microwave Studio software, with parameters chosen to be the best trade-off between computational resources and simulation accuracy. The outcomes from simulations allow both quantitative and qualitative approaches to the result analysis, and post-processing functions were developed to extract relevant KPIs.

The inputs for the model include antenna parameters, such as the gain, polarization or the antenna dimensions; and the environment parameters, in this case the longitudinal grooves and the higher placement of the antenna and ground plane, the ones that were changed to assess the results. Regarding the outputs, these come from the simulation results from CST: 2D and 3D radiation patterns, and other antenna metrics that would help to assess the performance of the system, such as the antenna gain, the half-power beamwidth, the main lobe direction, the reflection coefficient, and the first side lobe level.

First, the antennas were tested according to the set of parameters defined to validate them. Quarter-wave monopoles were used, with height tuned for correct performance. The ground plane size is set according to the minimum size defined in the datasheets of the commercial antennas considered for each of the frequencies (50x50 cm), except for the lower frequency, where a bigger ground plane is needed to achieve an acceptable reflection coefficient. The theoretical gain for λ/4 monopoles over an infinite ground plane is 5.19 dB, and the four antennas show a behavior according to the theory, with gains less than 1 dB different from the theoretical value, and acceptable reflection coefficients.

To assess the impact of the grooves, three different models were developed: a flat box of PEC to simulate a flat roof with no irregular surface, a straight roof featuring grooves, and a curved roof featuring grooves, these last two to simulate irregular roof surfaces, both in straight and curved configurations. Groove parameters are also defined since their size and spacing varies for different manufacturers and types of trains.

Three different approaches were considered, with a reference scenario common to all three: model of a train featuring a curved, grooved roof, with the antenna and ground plane placed 1 cm above the surface. The grooves for the reference scenario are medium-sized, according to the measurements (w_g=15 mm, h_g=25 mm, d_g=15 mm). The first approach tests the antennas for all the frequencies placed on the three 3D models; the second addresses the impact caused by the groove dimensions, comparing the reference scenario with simulations featuring a new model with wider grooves (w_g=25 mm, h_g=15 mm, d_g=20 mm); and the third, which consists in changing the height of the antenna and ground place in the reference curved groove scenario, in the interval $h_p \in [1; 20]$ cm , for which two additional heights were tested after the reference scenario (h_p=10 cm and h_p=20 cm).

In order to guarantee the link between the train-mounted antenna and the BS, some recommendations are drawn according to the results of the three different approaches:

- For 400 MHz systems the grooves do not impact significantly, but communications can be improved keeping the antenna close to the train roof;
- For 900 MHz systems, the addition of the grooves does not cause a gain loss, however increasing its height for h_p=20 cm improves the gain, hence doing so is recommended;
- For 2.6 GHz systems the strong impacts due to the grooved surface lead to the recommendation of adding a safety communications margin of 10 dB if an average approach is used, or 14 dB for the worst case approach (i.e. if vital systems depend on this link and the communication needs to be assured at any cost). It is, however, possible to reduce these margins if the antenna height is increased to 20 cm, and doing so the recommendation is to add a 7 dB safety margin only for the worst case approach;
- For 5.9 GHz systems grooved surfaces are also expected to generate strong impacts, and therefore a 5 dB safety margin should be considered as average approach, with 14 dB for the worst case approach. Being possible to increase the height of the antenna to 20 cm, then it is recommended to add a 10 dB margin only for the worst case approach.

REFERENCES

[1] L. Correia, *Mobile Communication Systems*, Slides, Instituto Superior Técnico, Lisboa, Portugal, 2018.

[2] *ERTMS history*, Factsheet, Association of the European Rail Industry, UNIFE, Brussels, Belgium, September 2018. [Online] Available in: (http://www.ertms.net/wp-content/uploads/2018/10/8-UNISIG1.pdf).

[3] GSM-R Operators Group, *Functional Requirements Specification Version 16.0.0,* European Integrated Railway Radio Enhanced Network, Paris, France, December 2015. [Online] Available in: (https://www.cept.org/files/18286/SRS-16.0.0%20UIC%20951-0.0.2.pdf).

[4] *Terrestrial Trunked Radio (TETRA) Release 2*, Technical Report, European Telecommunications Standards Institute, Sophia, France, October 2007. [Online] Available in: (https://www.etsi.org/deliver/etsi_tr/102500_102599/102580/01.01.01_60/tr_102580v010101p.pdf).

[5] *Broad Band Radio System (BBRS)*, Thales Group, Oeiras, Portugal, 2018.

[6] *Global Mobile Trends 2017 Report,* GSMA Intelligence, September 2017. [Online] Available in: (https://www.gsma.com/globalmobiletrends/index.html).

[7] *Installation Guidelines for Train and Bus Antennas*, Technical Guide, Version 1.0, Kathrein SE, Rosenheim, Germany, 2002. [Online] Available in: (http://www.kathrein.fr/media/installation_guide_for_train_antennas.pdf).

[8] *Installation instruction for train and bus antennas (outdoor)*, Technical Guide, Antonics-ICP GmbH, Velten, Germany. [Online] Available in: (https://www.antonics.com/fileadmin/antonics/img/Bilder/technische-Informationen/Installation_instruction_train_and_bus_antennas_EN.pdf) [Accessed in December 2018].

[9] R. Parameswar, P. Rao, K. Ray, N. Balakrishnan, "Analysis of distributed conformal antennas on a moving platform", SAMEER – Centre for Electromagnetics, Indian Institute of Science, Bengaluru, India, 2011. [Online] Available in: (https://ieeexplore.ieee.org/stamp-/stamp.jsp?arnumber=6256843).

[10] V. Pals, *Analysis of influence of antenna radiation patterns by conducting environments for the development of vehicle antennas,* M.Sc. Thesis, Technische Universität München, Munich, Germany, 2013.

[11] D. Williams, *Train Roof Antenna Positioning Issue Study,* T739 Project, Rail Safety and Standards Board (RSSB), Siemens Mobility UK, United Kingdom, July 2009. [Online] Available in: (https://www.rssb.co.uk/research-development-and-innovation/research-project-catalogue/t739).

[12] A. Ribeiro, *Analysis of Antenna's Locations on Trains for Mobile Communications*, M.Sc. Thesis, Instituto Superior Técnico, Lisbon, Portugal, 2018.

[13] E. Teoh, *Train roof*, Malaysia, 2009. [Online] Available in: (https://www.flickr.com/photos/monkey-ed/4120777067).

[14] J. Soure, *Implementação do Sistema GSM-R na Rede Ferroviária Nacional – Projeto-piloto*, M.Sc. Thesis, Instituto Superior de Engenharia de Coimbra, Coimbra, Portugal, 2013. [Online] Available in: (https://comum.rcaap.pt/handle/10400.26/13547).